2

CONF-930930--1

WSRC-MS-92-362

FLOW REGIME MAPPING OF VERTICAL TWO-PHASE DOWNFLOW IN A RIBBED ANNULUS (U)

by A. L. Kielpinski

Westinghouse Savannah River Company
Savannah River Site
Aiken, South Carolina 29808

Other Authors:

MASTER

A paper proposed for Presentation/Publication
at/in the National Heat Transfer Conferene
Atlanta, GA
08/08-11/93

DISCLAIMER

FLOW REGIME MAPPING OF VERTICAL TWO-PHASE DOWNFLOW IN A RIBBED ANNULUS

A. L. Kielpinski

Savannah River Technology Center

Westinghouse Savannah River Company

Aiken, South Carolina 29808

FLOW REGIME MAPPING OF VERTICAL TWO-PHASE DOWNFLOW IN A RIBBED ANNULUS

A. L. Kielpinski

Savannah River Technology Center

Westinghouse Savannah River Company

Aiken, South Carolina 29808

ABSTRACT

Two-phase flow regimes have been mapped for vertical, cocurrent downflow in a narrow annulus which is partially segmented by the presence of longitudinal ribs. This geometry and flow condition has application to the analysis of a Large-Break Loss of Coolant Accident (LB-LOCA) in the production K-Reactor at the Savannah River Site (SRS). The ribbed annular geometry, particularly the presence of non-sealing ribs, gives rise to some unique phenomenological features.

The flow behavior is influenced by the partial segmentation of the annulus into four quadrants or subchannels. The segmentation is partial because of the imposed clearance between the rib circle and the surrounding tube. A random element is introduced by the natural bowing of the slender tubes; the width of the azimuthal flow path between two subchannels at a given axial location is indeterminate, and can take on any value between zero and the maximum clearance (nominally 7.6×10^{-4} m). When the rib gap is zero at a given location, it is at a maximum 180° away at the same axial location. Therefore, the

range of rib gaps is spanned in a single test section, as it would be also in a reactor assembly.

As a result of these effects, flow regime maps obtained by other researchers for downflow in annuli are not accurate for defining flow regimes in a ribbed annulus. Flow regime transitions similar to those noted by, e.g., Barnea[1], were observed; the locations of these transitions, however, were displaced with respect to the transition equations derived by Barnea[1]. Moreover, for the integral observations made in this experiment, wherein the flow regime of the entire test section is of interest, the existence of subchannel interaction is associated with observations which do not easily fit into the flow regime transition framework. Because the subchannels are in partial and somewhat irregular communication, small azimuthal pressure differences can be set up at one axial location (where the rib gap is small) which drive flow across the rib at a downstream location (where the rib gap is larger). As a result, multiple flow regimes were simultaneously observed under certain flow conditions.

Experimental bubble rise velocity measurements were also obtained in the same test section. The bubble rise velocities were much higher than expected from the theory developed for slug bubbles in tubes, unribbed annuli, and rectangular channels[2,3]. The rise velocity data were in much better agreement with the predictions of Grace and Harrison[4] for two-dimensional elliptical-cap bubbles. An elliptical-cap bubble rises faster than a slug bubble of the same area. Large, slug-shaped bubbles injected into the test section were observed to reduce in size as they rose, due to interaction with a longitudinal rib. They thereby adopted a shape more like an elliptical-cap bubble, hence rising faster than the original slug bubble would have risen.

Flow Regime Mapping for Vertical Downflow in a Ribbed Annulus

I. INTRODUCTION

Thermal-hydraulic behavior in two-phase flows is a function of the qualitative, geometric configuration of each phase--the flow regime. A flow regime map, indicating what configuration the two-phase flow is in for a given combination of independent variables, is necessary in order to make use of regime-dependent analytical or empirical models. Because of their fundamental nature and their practical application in the commercial nuclear, chemical, and petroleum industries, both horizontal pipe flow and vertical upward pipe flow have been extensively studied[5]. A more limited amount of research on vertical downward pipe flow and on flow in non-circular geometries is available[1,6,7]. Because the direction of flow and the geometry of the channels can influence the mechanisms of bubble formation, coalescence, etc., different flow configurations may have unique flow regimes. For example, stratified flow in horizontal pipes has no counterpart in vertical pipe flow.

The geometry of the Savannah River Site (SRS) reactor assemblies is that of nested, longitudinally-ribbed cylinders (Figure 1). The resultant flow passages within the assembly are partially segmented annuli. The quadrants ("subchannels") of one of these annuli, defined as the 90° sector bounded by two ribs, constitute parallel paths which are in partial communication. In practice, the precise degree of communication at a given location is unknown; the nominal 0.012-cm diametral gap which exists between the rib circle of one cylinder and the surface of the neighboring cylinder varies with location and time, due to random bowing of the long, slender cylinders. The ribs will touch the adjacent cylinder at random locations. At such points of rib contact, neighboring quadrants, or subchannels,

are isolated from one another, while the two subchannels 180° away are at maximum communication. Such rib contact is not expected to occur over the full axial length. Thus, quadrants which are isolated from one another, and sustaining an azimuthal pressure difference at one axial location, may be in communication at another axial level.

The geometry so described has not been extensively studied, and presents some unique features which can and do influence thermal-hydraulic behavior. In particular, the partial segmentation of the annuli and the varying degree of communication which can exist between subchannels gives rise to behavior which is unlike either of the geometrically-limiting cases, i.e., unribbed annuli or thin rectangular channels. This paper reports on a study of flow regimes in a ribbed annulus geometry, under air-water downflow over ranges applicable to the analysis of the emergency cooling system (ECS) phase of a large-break, loss of coolant accident (LOCA).

II. EXPERIMENTAL SETUP AND INSTRUMENTATION

The experimental setup is shown in Figure 2, with test section dimensions as given in Table 1. The ribbed annulus was formed using an extruded, ribbed lithium-aluminum cylinder (an unirradiated component of an SRS assembly) surrounded by precision-bore glass. Glass was chosen to ensure visibility, while preserving the surface wettability characteristic of the aluminum oxide layer which forms on the prototypical outer cylinder. The glass was segmented, with aluminum flanges interspersed at regular intervals. Pressure taps, 0.32 cm in diameter, were drilled into the aluminum flanges to allow axial pressure profiles to be measured in one subchannel of the ribbed annulus. The inner

diameter of the flanges was machined to the same diameter as that of the glass, and there was no evidence that flow was interrupted by geometric discontinuities.

The flow in the ribbed annulus, the test section proper, exited into an unribbed annulus, passed through a set of holes, of diameter 0.64 cm, in the outer cylinder of the latter, and thence into an outlet tank. The geometric features of the outlet were included to simulate the prototypical outlet geometry of an SRS reactor assembly, but are not believed to influence the flow regime as a function of mass fluxes or of pressure drop.

Water and air were introduced separately into each of the four subchannels. To ensure even distribution over the surfaces, the water was introduced by means of a bank of 44 tubes, each of diameter 0.132 cm; the air was introduced into 16 holes of diameter 0.366 cm. Individual subchannel water flows were measured by means of rotameters, each of 1.74×10^{-4} m^3/s full scale and with an estimated uncertainty of 1% full scale. The total airflow was measured by means of an electronic mass flowmeter (Omega®, 8.33×10^{-4} m^3/s full scale, with maximum estimated uncertainty of 3.3×10^{-5} m^3/s). Similar flowmeters were installed on each subchannel, for redundancy and to assist in regulating an even distribution of air flow. Electronic pressure transducers (1.724×10^5 Pa full scale, maximum uncertainty 6.8×10^3 Pa), were used to monitor pressures at several axial locations. All electronic readings were taken at 1 Hz using a Macintosh II®-based data acquisition system, using the commercially-available Strawberry Tree Workbench® software. The values reported are time-averages of such readings taken over intervals of 30-60 seconds.

The test section was also used to acquire measurements of a rising bubble in a stagnant liquid. To make these measurements, a volume of air was introduced into the bottom of the water-filled annulus, through a tap (0.32-cm diameter) in the bottom-most

aluminum flange. The time taken to traverse an axial length of 2.54 m was measured with a calibrated stopwatch.

The volume and length of the bubbles were measured as follows. The bubble volume was measured by introducing the air via a volume-calibrated syringe. The bubble, along with a measurement scale, was videotaped with a shutter speed of 1/1000 seconds. The length of the bubble was then measured from the videotape frame.

The instrumentation was calibrated before and after the testing period. Daily zero checks were acquired for the pressure and airflow instrumentation.

III. TEST PROCEDURE

The tests were arranged in series of ascending or descending values of one of the independent variables, i.e., the air or water flowrate. The other flowrate was then held constant throughout the series. In this way, hysteresis effects could be examined. Each test series was started from a water-solid condition. This ensured a uniform initial condition for all test series.

For all of the data reported here, the water flow was equally distributed to the four subchannels. At low air flows, it was difficult to achieve uniformity in the individual subchannel airflows. As discussed below, however, mass transfer past the ribs tends to drive an initially uniform distribution to a non-uniform one. Because of this, the inlet subchannel flows are not necessarily representative of the true local flow conditions. Therefore, the flow map is best characterized in terms of annulus-averaged values of the air and water flowrates.

Flow regimes were assessed visually. Prior to the mapping effort, the range of conditions was explored in order to ascertain the different flow regimes which would be encountered. To ensure consistency in the reported observations, a compendium of the various observed flow conditions was compiled on videotape for use as a reference during the test program. Testing conditions were likewise recorded on videotape. All taping was done at a shutter speed of 10^{-3} s.

Having controlled both the air and liquid flowrates, the flow regime in the main body of the test section was determined as a function of the flowrates and the direction of the test series (i.e., ascending gas flow, descending gas flow, ascending water flow, or descending water flow).

Bubble rise velocities were made using a calibrated stopwatch and measuring the time necessary to traverse a 2.54 m distance. The bubbles were introduced into a port located in the center of one subchannel, near the bottom of the annulus. The bubbles were injected either by a squeeze bulb, wherein no direct volume measurement could be made, or via a calibrated syringe, which provided a volume measurement. The bubbles were recorded on videotape, as described previously.

IV. FLOW REGIMES IN RIBBED ANNULUS DOWNFLOW

Flow regime mapping is subject to considerable semantic confusion. Spedding and Nguyen[8] define droplet, annular, slug, bubble, and pulsating froth regimes in vertical cocurrent downflow (with some combinations of these as well). Barnea et al.[9] use the terms dispersed bubble, slug, and annular for this flow orientation. In initial observations

of the present test section, the following types of flow were produced: bubble (small spherical bubbles), slug (capped bubble), churn-turbulent (upward as well as downward motion of irregularly shaped bubbles), wavy-annular (rippling films), annular (smooth films), and rib flow (i.e., flow almost exclusively down the ribs rather than the other annular surfaces).

Because the four subchannels are in partial and somewhat irregular communication, due to the varying rib gaps set up by the bowing tubes, small azimuthal pressure differences can be set up at one axial location (where the rib gap is small) which drive flow across the rib at a downstream location (where the rib gap is larger). This "wandering" of flow is quite characteristic of ribbed annulus flow, and has been observed using heat as a tracer[10].

The mass transfer across the rib gaps leads to another flow phenomenon, not seen in other geometries, which is associated with the crossflow process itself. Where liquid crossflow occurs, the azimuthal jet breaks up any large bubbles found in the receiving subchannel, and there is a local region of bubbly flow, regardless of overall flow conditions. It is not clear whether the bubbly flow observed is mainly due to breakup of the gas bubbles in the receiving channel, or due to gas transfer across the rib as well. Observation shows that there is a film on the rib itself, regardless of overall flow regime; this film is generally thicker than that on the other surfaces when an annular flow is present. Therefore, while gas transfer probably occurs, it is likely that the void fraction of the crossflow is considerably less than the annulus-averaged void fraction.

The local departures from average conditions complicate the flow regime observations considerably, since the flowrates are not controlled or measured on a local scale. The liquid subchannel flowrates typically span the range 15-35% of the total flow

(i.e., with 25% denoting uniformity)[11]. The range of variation of local airflows has not been characterized to date.

The effect of this situation is that, over much of the test range, two (or more) distinct flow regimes can be observed in adjacent subchannels, or in the same subchannel at different axial locations. The effect exacerbates the natural "fuzziness" of flow regime transition lines; not only may a given combination of gas and liquid flowrates be in the transition region, but individual subchannels may have less or more flow than the nominal flow settings would indicate. Early efforts to map flow regimes in a detailed fashion were greatly complicated by this phenomenon; attempts to note down the flow regime at many locations in the rig became cumbersome.

The mapping technique which was finally used was simply to determine flow regime which best described the overall behavior of the main portion of the test section. Because the entrance region behavior was affected by the mode of introduction of the two components, the topmost section of the test section (i.e., between the inlet flange and the first aluminum instrumentation flange) was considered separately. Since some two-phase flow regimes may in themselves be considered developing flows, as suggested by Taitel et al.[5], this consideration of an arbitrary length as constituting the development region is necessarily crude, but it proved reasonable in practice.

The three regime classifications used in this study were defined as follows:

- Bubbly: Liquid is the continuous phase, with spherical, spherical-capped, or short bullet-shaped bubbles flowing downward. Although not a requirement in the working definition, the bubbles observed in this regime generally were smaller than the azimuthal width of a subchannel.

- Churn: Large, irregularly-shaped bubbles which break up and coalesce and which appear to alternate direction or to remain stationary for as much as several seconds. A primary distinction between this and the bubbly regime described above is the oscillatory nature of both the air and the liquid flow.

  Taitel et al.[5], in discussing upflow, refer to the churn regime as development-length behavior which culminates in slug flow. Long Taylor bubbles are not easily sustained in ribbed annulus cocurrent downflow, however. Hence, the region of true slug flow is narrow, perhaps nonexistent; when long bubbles form, they are broken up as described and churn flow results.

- Annular flow: Liquid films flow on the walls and ribs, while a gas core forms in the center of each subchannel. Such a configuration results either when the inlet pressure is atmospheric, with zero airflow and low liquid flowrates, or at positive inlet pressures, with high airflow. The film on the ribs appears thicker than that on the other surfaces. If the liquid flowrate is low enough, the flow is almost exclusively on the ribs.

Transition flows between these main regimes (e.g., churn-bubbly) were also noted. One exception was made to the practice of characterizing the main body of the test section by a single regime. In some tests, distinctly different flow regimes were exhibited by the different subchannels over the whole axial length. In many cases, all three of the main

flow regime classifications were observed concurrently in neighboring subchannels. That is, rather than all four subchannels exhibiting a common flow regime which is qualitatively intermediate between, say, churn and annular, one subchannel might be completely in churn flow, adjacent to one completely in annular flow, perhaps with the remaining two channels in bubbly flow. When this type of behavior was noted, the regime was denoted as "mixed." A limited amount of repeated runs indicated that the "mixed" behavior was repeatable.

V. EXPERIMENTAL RESULTS: FLOW REGIME MAPPING

The experimental results are plotted, with superficial velocities as the coordinates, in Figure 3. Lines are drawn in to represent approximate flow regime boundaries. No distinction has been made in this plot between the four different test series, i.e., constant water flow, ascending air flow; constant water flow, descending air flow; constant air flow, ascending water flow; and constant air flow, descending water flow.

Several features are notable in Figure 3. A bubbly-annular transition is observable where the three main flow regimes meet. The "mixed" flow behavior occurs in this region, as well as occurring in the middle of the churn flow regime. This mixed-flow behavior is repeatable, as evidenced by the pairs of points at superficial gas velocities of 0.5-0.6 m/s. Also notable is the presence of a bubbly/annular transition. Bubbly-annular behavior is also observable along the annular to churn transition, which occurs around liquid velocities of 0.3 m/s. In the latter instance, the bridging of the liquid film was accompanied by the formation of bubbles, without the oscillatory motion associated with the churn regime. This behavior may be indicative of the slug flow regime which appears to be largely suppressed in ribbed annular two-phase downflow.

In Figure 4, the flow regime map is decomposed into four maps, according to the type of test series from which the points were derived. This enabled the identification of hysteresis effects. Due to limitations in the air supply, the superficial gas velocity changed somewhat between tests in some series intended to be at constant air flow (though gas flow was constant during each individual test); points constituting a test series should be obvious, however. From this figure, we see that the bubbly-annular flow observed at a liquid velocity of about 0.3 m/s only occurred when the liquid velocity was held constant at that value; it did not occur when air flow was held constant. It was, however, observable both at increasing and decreasing airflows.

Figure 4 also shows that the "mixed" flow regime, wherein distinct flow regimes were observed in different subchannels, occurred primarily when the liquid flow was varied. In particular, this phenomenon was observed mainly when the water flow was increased during the course of the test series. That the "mixed" regime was reproducible is shown by the pairs of points for $0.5 < j_g < 0.6$ m/s. It is not clear that the behavior would have been observed at these conditions for a descending air flow series.

VI. COMPARISON WITH OTHER MAPS

It is of interest to compare the flow regime map with that obtained by other researchers for adiabatic two-phase downflow. Most of the available data are for tubes. Figure 3 contains the flow transitions derived by Barnea and by Barnea et al.[1,8], which compared favorably for air-water downflow in a 2.54 cm tube at pressure and temperature conditions similar to those of the present study. Barnea employed three flow regime definitions--annular, intermittent (i.e., churn or slug), and dispersed bubbly. Barnea's annular-churn transition reduces to:

$$\alpha \geq 0.76$$

(1)

As will be shown below, void fraction can be estimated from the experimental data. The plotted transition line agrees well with the flow regime observations.

Barnea's transition from churn to bubbly flow is somewhat at variance with the ribbed annulus results. Barnea's transition criteria are based on three physical arguments. First, at liquid rates low enough that turbulent breakup of bubbles is low, a bubble-to-slug transition of $\alpha = 0.25$ is offered on the grounds that this is about half the value of maximum packing for a cubic lattice. Second, it is argued that, above a critical bubble diameter, bubble deformation occurs, thereby enhancing bubble coalescence and the transition to slug or churn flow. This critical diameter is estimated as twice the diameter below which bubbles act as solid spheres; it is known that the latter is a lower bound to experimental observation. The third criterion is that bubbly flow cannot exist above the maximum-packing value of void fraction; Barnea et al. select $\alpha = 0.52$ as the maximum value, based on a cubic lattice (although selection of other lattice configurations leads to varying values; Ishii calculated $\alpha = 0.60$ by similar arguments).

The resultant transition line lies above the data. However, if the estimate of critical diameter for coalescence is increased by 50%, and if the maximum-packing void fraction is of the order of 0.60, Barnea's transition criteria can successfully predict the observed bubbly flow points shown in the figure. The critical bubble diameter is considered to be that above which the bubble is deformed, and the rise velocity is constant. The need for an increased estimation of critical bubble diameter to extend Barnea's transition criterion to the present case is consistent with the general observation that the bubble rise velocity in a ribbed annulus differs from that in a tube. This will be discussed further later in this report.

In an earlier study, Spedding and Nguyen[9] presented a flow regime map for air-water, tubular, vertical downflow in terms of the dimensionless parameters Q_l/Q_g and a Froude number. The tube used in their study was 4.55 cm in diameter. Figure 5 compares the present results with those of the earlier study. The range of the present work just grazes the bubble-slug transition line of Spedding and Nguyen. No bubbly flow was observed near their transition, however; the small region of bubbly flow obtained in the present study occurs well into the annular+slug region of Spedding and Nguyen. The purely annular regime given by these authors occurs at much lower values of Q_l/Q_g than the experimental results of the present study.

The discussion of analytical transition criteria showed the need for void fraction information. The emphasis on two-fluid modeling, e.g., in nuclear reactor thermal-hydraulic safety analyses, also makes it desirable to cast the flow regime map in terms of void fraction vs. mass flux. Void fraction was not experimentally measured in the present study. The pressure drop data, along with the air and water flow measurements, can be employed to estimate the void fraction, however. Consider a simplified, one-dimensional mixture momentum balance in the axial direction:

$$0 = -\frac{dp}{dz} + \left[\alpha\rho_g + (1-\alpha)\rho_f\right]g - F_w^z \qquad (2)$$

The wall drag term is given in terms of a friction factor, f:

$$F_w^* = \frac{1}{2}\frac{f(\mathrm{Re})\rho_f|u_f|u_f}{D_h} = \frac{1}{2}\frac{f(\mathrm{Re})\rho_f|j_f|j_f}{D_h(1-\alpha)^2} \tag{3}$$

where the Reynolds number is defined as:

$$\mathrm{Re} = \frac{\rho_f|u_f|D_hK_h}{\mu_f} = \frac{\rho_f|j_f|D_hK_h}{\mu_f(1-\alpha)} \tag{4}$$

with K_h, a hydraulic diameter correction factor, given by Blevins[12]. For the present test section, K_h is equal to 0.796.

Given a friction factor relationship, the pressure gradient, and the flowrates, the void fraction can be computed by substituting (3) into (2). Since the resulting equation is cubic in void fraction, the void fraction estimation is not too sensitive to the exact form of the friction factor. A single-phase friction factor model has been found to be sufficiently accurate to yield excellent predictions of void fraction[13]. Thus, the void fraction in the present test section was estimated using experimental data and the following model for the friction factor:

$$f_l = 64 / \mathrm{Re} \qquad \mathrm{Re} < 2000 \tag{5a}$$

$$f_t = \left[1.14 - 2\log_{10}\left(\frac{\varepsilon}{D_hK_h} + \frac{21.25}{\mathrm{Re}^{0.9}}\right)\right]^{-2} \qquad \mathrm{Re} > 4000 \tag{5b}$$

$$f_{l-t} = \left(2 - \frac{4000}{\mathrm{Re}}\right)\left[f_t(\mathrm{Re}=4000) - f_l(\mathrm{Re}=2000)\right] + f_l(\mathrm{Re}=2000)$$

$$2000 \le \mathrm{Re} \le 4000 \quad (5c)$$

Equations (5a) and (5b) are standard representations of laminar and turbulent single-phase friction factors for a tube, modified for an annulus through use of the factor K_h, while equation (5c) is a linear interpolation between them. Equation (5a) can be derived analytically (as done many standard texts, e.g., John and Haberman[14]); equation (5b) is an explicit approximation to the Colebrook-White equation.

With void fraction estimated by the above method, Figure 6 presents the flow map in terms of the parameters void and mass flux. Also shown for comparison are the transitions given by Ying and Weisman[15] for adiabatic, two-phase downflow of refrigerant 113 in a 2.54 cm tube. Once again, the ribbed annulus data deviates from the transitions given for tube flow. It is noteworthy that, in these coordinates, the test matrix (which represents the conditions of interest for the LOCA analysis) collapses into a fairly narrow band which nonetheless spans the flow regime transitions.

VII. BUBBLE RISE VELOCITY MEASUREMENTS

Figure 7 shows the rise velocity in the ribbed annulus of single bubbles in stagnant liquid, as a function of bubble length. The most notable feature of the plot is the presence of rise velocities of 0.55 m/s or more. Such values are significantly higher than

those observed in tubes, rectangular sections, or unribbed annuli, as discussed further below.

Upon injection into the stagnant column of water, larger bubbles tended to break up, either immediately upon injection or later, during the bubble traverse up the annulus. The immediate breakup of the bubble is believed to account for the several outlying points in data set 2. It was found that injected bubbles of length greater than 2.9 cm (about 3 ml volume) also tended to break up as the bubble rose, however. This latter type of breakup was gradual and continual, a kind of shearing off of small, spherical bubbles from the original spherical-cap or bullet-shaped bubble. The breakup occurred as the bubble veered azimuthally during its rise, encountering a longitudinal rib in passing. Such breakup appeared to commence sooner with larger initial bubble size, and appeared to continue during the subsequent traverse. The experimental setup did not permit measurement of the final bubble size. Since the bubble continued to decrease in size as it rose, the final bubble size is dependent on the overall length of the test section. From the visual observations, however, it appeared that the final length was approximately 3 cm--i.e., the maximum size which was able to rise without breakup.

Given the trend of smaller bubbles to rise more slowly, then, the data of Figure 7 for bubbles above 2.9 cm must represent a lower bound to the true rise velocity, since the rise velocity of an ever-shrinking bubble was in fact what was measured. In view of this limitation in the measurements, then, the high values of rise velocity are even more striking. Bubble rise velocities have been expressed as[2,3]:

$$V_b = K\sqrt{gD} \tag{6}$$

where V_b is the rise velocity of a bubble in a stagnant medium, and D is the characteristic length of the channel. For a tube, D is the tube diameter, and the value of the coefficient K ranges from 0.32 to 0.36[2]. The simplest extension of the basic formulation to non-circular channels is then to replace D by D_h, the hydraulic diameter. This choice has proved unsuitable, however. Griffith[2] proposed using the outer diameter D_o for an annulus, or the wide dimension of a rectangular channel, and was thus able to obtain values of K for those geometries which were of approximately the same range as those obtained for tubes. More recently, Sadatomi et al.[6] proposed an equi-periphery length, but without a firm theoretical basis. Barnea and Shemer[16] used the original reasoning of Davies and Taylor[17], i.e., that the characteristic diameter is that of the bubble nose, to derive a more complicated function based on the fact that two radii of curvature exist for a bubble in an annular geometry. Their expression is

$$D = \frac{1}{2}\left[\frac{\pi(D_o + D_i)}{2} + \frac{(D_o - D_i)}{2}\right] \tag{7}$$

i.e., the average of the two radii of curvature, where each radius of curvature is approximated by the relevant dimension of the channel. Note that for narrow annuli (D_o - D_i small), the expression reduces to one-half the average circumference of the channel. An extension to the model of Barnea and Shemer is more suitable for a ribbed annulus. The first term in brackets in Eq. (6) approximates the large radius of curvature by the circumference of the annulus. While this is appropriate for an axisymmetric bubble in an unribbed annulus, it will be in error for an asymmetric bubble. For the present case, the bubble is confined by the ribs to a 90° sector (if it is to remain intact), so the first term in brackets should be divided by four.

Given a maximum experimental value of ≈ 0.55 m/s for V_b obtained in the present experiment, one can compute a value of K using any of these prescriptions for characteristic length. Table 2 summarizes the results for various model choices for D. It is obvious that the value of K so derived exceeds the expected range significantly. Defining the characteristic dimension by treating the subchannel as a rectangular channel does not change this conclusion.

An analysis of two-dimensional elliptical-cap bubbles in inviscid liquid was performed by Grace and Harrison[18], with circular-cap and parabolic-cap bubbles as limiting cases of zero eccentricity and infinite focal length, respectively. A brief summary of their results is as follows:

The rise velocity of elliptical bubbles is given by:

$$V_b = c_2\sqrt{g\sqrt{A_b}} \tag{8}$$

where V_b is the rise velocity, A_b is the area of the (planar) bubble, and c_2 is given by

$$c_2 = \left[\frac{2m}{f(\gamma)}\right]^{0.25} \frac{\sqrt{\gamma}}{\left[2m\sqrt{2\gamma-1}+1\right]} \tag{9}$$

Here m = h/l, the ratio of bubble height to span, γ is the ratio of the major axis of the ellipse to the height of the bubble, and $f(\gamma)$ is given by:

$$f(\gamma) = \frac{\gamma^2}{\sqrt{2\gamma - 1}} \cos^{-1}\left(\frac{\gamma - 1}{\gamma}\right) - (\gamma - 1) \tag{10}$$

The area of the bubble, A_b, is given in terms of the bubble height and span by

$$A_b = \frac{h^2 f(\gamma)}{2m} = \frac{hl}{2} f(\gamma) \tag{11}$$

The analysis is limited to $\gamma > 0.5$, to avoid division by zero in equation (9).

Bubble rise velocities were computed using Grace and Harrison's model. The best comparison was achieved by choosing the limiting case of $\gamma \rightarrow 0.5$ (specifically, γ = 0.501) and using the experimentally-measured bubble dimensions. (Curiously, this choice of γ yields results which are virtually identical to those obtained by Grace and Harrison for the rise velocity of a large, isolated circular-cap bubble, even though the latter result presumes a value for m which is inconsistent with the present data.) The results are shown in Figure 7. The agreement is rather good, particularly at the higher rise velocities and in contrast to the models for slug bubbles discussed earlier.

At 2.9 cm (the maximum length without bubble breakup), the bubbles approximately span the circumference of the 90° annular sector (0.036 m, based on a diameter midway between inner and outer). The presence of the longitudinal ribs is thus felt in this range. Given this, these smaller bubbles are not really "slug" bubbles, if the latter implies a bubble height which is significantly greater than the channel span, and for which wall effects predominate. Grace and Harrison noted that an elliptical

(unconstrained) bubble rises faster than a slug bubble of the same area. Based on the agreement of the data with the elliptical model, it appears that the latter model is more appropriate. We speculate that the longer bubbles, though subject to the "shearing" mechanism described above, continue to act as if unconstrained by the longitudinal ribs.

VIII. CONCLUSIONS

Flow regimes have been mapped for a ribbed annulus in two-phase downflow. The results have been compared to data for downflow in other geometries. Although the general regime classifications hold, the regime boundaries differ somewhat from those of the other geometries. Moreover, the partial segmentation of the flow paths induced by the longitudinal ribs gives rise to some unique phenomenological behavior, such as the bubbly flow associated with rib crossflow. The rise velocities of bubbles in the ribbed annular geometry are high when compared to those of slug bubbles in other geometries. The measured velocities compare favorably with those predicted for two-dimensional bubbles whose curvature is described by an ellipse of major axis one-half the height of the bubble.

IX. ACKNOWLEDGEMENTS

The information contained in this article was developed during the course of work under Contract No. DE-AC09-89SR18035 with the U. S. Department of Energy. The staff of the Experimental Thermal-Hydraulics Group and the Heat Transfer Laboratory of the Savannah River Technology Center were instrumental in carrying out this experiment. G. P. Flach and J. L. Steimke provided helpful discussion.

NOMENCLATURE

D_h hydraulic diameter

$\frac{dp}{dz}$ pressure gradient

f friction factor

F_w^z wall drag in the axial direction

g acceleration due to gravity

j_f superficial liquid velocity

j_g superficial gas velocity

K_h hydraulic diameter correction factor

m ratio of bubble height to bubble span

Re Reynolds number

u_f liquid velocity

V_b bubble rise velocity

α void fraction

δ falling film thickness

γ ratio of major axis of ellipse to bubble length

μ viscosity

ρ density

τ_w wall shear stress

REFERENCES

1. Barnea, D., "A Unified Model for Predicting Flow-Pattern Transitions for the Whole Range of Pipe Inclinations," Int. J. Multiphase Flow, **13** (1987).

2. Griffith, P., "The Prediction of Low-Quality Boiling Voids," ASME Trans., J. Heat Transfer, **86** (1964).

3. Wallis, G. B., One-Dimensional Two-Phase Flow, McGraw-Hill, New York (1969).

4. Grace, J. R., and Harrison, D., "The Influence of Bubble Shape on the Rising Velocities of Large Bubbles," Chem. Eng. Sci., **22**, (1967).

5. Taitel, Y., Bornea, D., and Dukler, A. E., "Modelling Flow Pattern Transitions for Steady Upward Gas-Liquid Flow in Vertical Tubes," AIChE J., **26** (1980).

6. Sadatomi, M., Sato, Y., and Saruvatari, S., "Two-Phase Flow in Vertical Noncircular Channels," Int. J. Mult. Flow, **8** (1982).

7. Kelessidis, V. C., and Dukler, A. E., "Modeling Flow Pattern Transitions for Upward Gas-Liquid Flow in Vertical Concentric and Eccentric Annuli," Int. J. Mult. Flow,**15** (1989).

8. Spedding, P. L., and Nguyen, V. T., "Regime Maps for Air Water Two Phase Flow," Chem. Eng. Sci., **35** (1980).

9. Barnea, D., Shoham, O., and Taitel, Y., "Flow Pattern Transition for Vertical Downward Two Phase Flow," Chem. Eng. Sci., **37** (1982).

10. Steimke, J. L., 1988, "Status of Heat Transfer Experiment (U)," E. I. DuPont de Nemours Technical Report DPST-88-854.

11. Whatley, V., 1987, "Subchannel Flow Distribution Measurements in Fuel Assemblies at ECS Flow," E. I. DuPont de Nemours Technical Report DPST-87-662.

12. Blevins, R. D., 1984, Applied Fluid Dynamics Handbook, Van Nostrand Reinhold, New York.

13. Flach, G. P., ed., "FLOWTRAN-TF Software Design (U)," Westinghouse Savannah River Company Technical Report WSRC-TR-92-532, Revision 0 (1993).

14. John, J. E. A., and Haberman, W. L., Introduction to Fluid Mechanics, New Jersey: Prentice-Hall (1971).

15. Ying, A., and Weisman, J., 1989, "The Relationship Between Interfacial Shear and Flow Patterns in Vertical Flow," Int. J. Multiphase Flow, Vol. 15, pp. 23-34.

16. Barnea, D., and Shemer, L., "Rise Velocity of Large Bubbles in Stagnant Liquid in Noncircular Ducts," Int. J. Mult. Flow, **12** (1986).

17. Davies, R. M., and Taylor, G. I, "The Mechanics of Large Bubbles Rising Through Extended Liquids and Through Liquids in Tubes," Proc. R. Soc., Series A, **200** (1950).

18. Grace, J. R., and Harrison, D., "The Influence of Bubble Shape on the Rising Velocities of Large Bubbles," Chem. Eng. Sci., **22** (1967).

Table 1

Test Section Dimensions

Annulus Outer Diameter [cm]	5.08
Annulus Inner Diameter [cm]	4.04
Annulus Length [cm]	411.5
Nominal Diametral Rib Gap [cm]	0.08
Hydraulic Diameter [cm]	0.87
Cross-Sectional Flow Area [cm^2]	7.14
Distance between Pressure Taps [cm]	78.7

Table 2. Comparison of Various Models to Experiment.

Form for D	Reference	K: Model	K: Expt.
$D=D_h$	Extension from tube results	0.32-0.36	1.85
$D=D_o$	Griffith, 1964	0.35-0.43	0.78
$D = \frac{\mathcal{P}}{\pi}$	Sadatomi et al., 1982	0.31-0.39	0.54
$D=\frac{1}{2}\left[\frac{\pi(D_o+D_i)}{2}+\frac{(D_o-D_i)}{2}\right]$	Barnea and Shemer, 1986	0.35	0.65
$D=\frac{1}{2}\left[\frac{\frac{\pi}{4}(D_o+D_i)}{2}+\frac{(D_o-D_i)}{2}\right]$	Extension to Barnea and Shemer	0.35?	1.22

Figure 1

Cross-Section of SRS Reactor Assembly

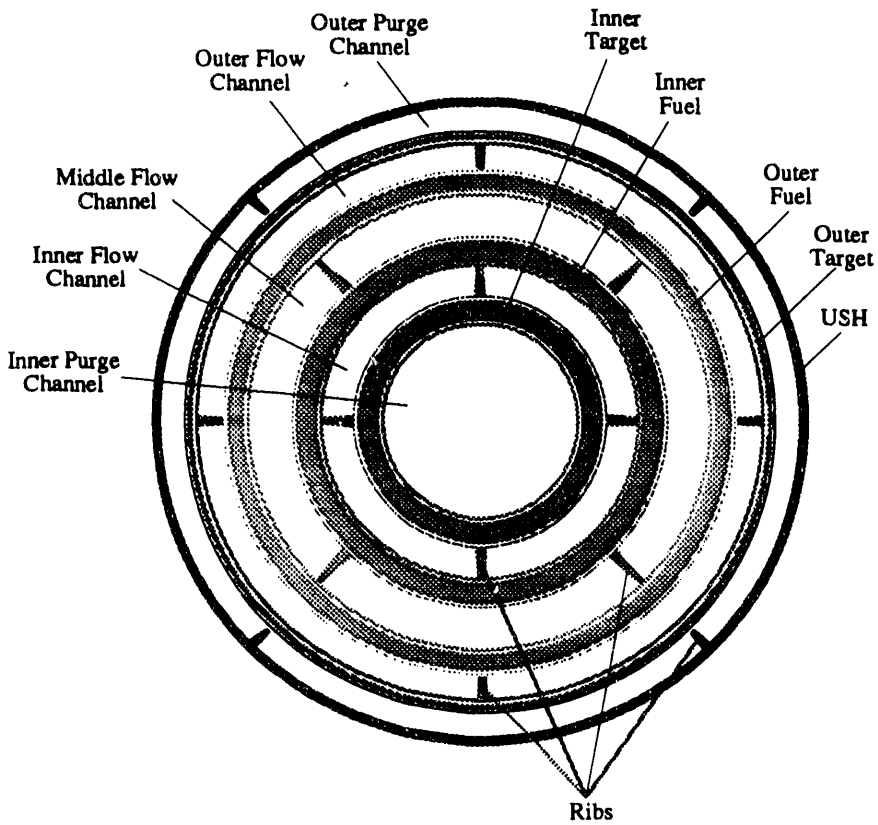

FIGURE 2
LOOP SCHEMATIC

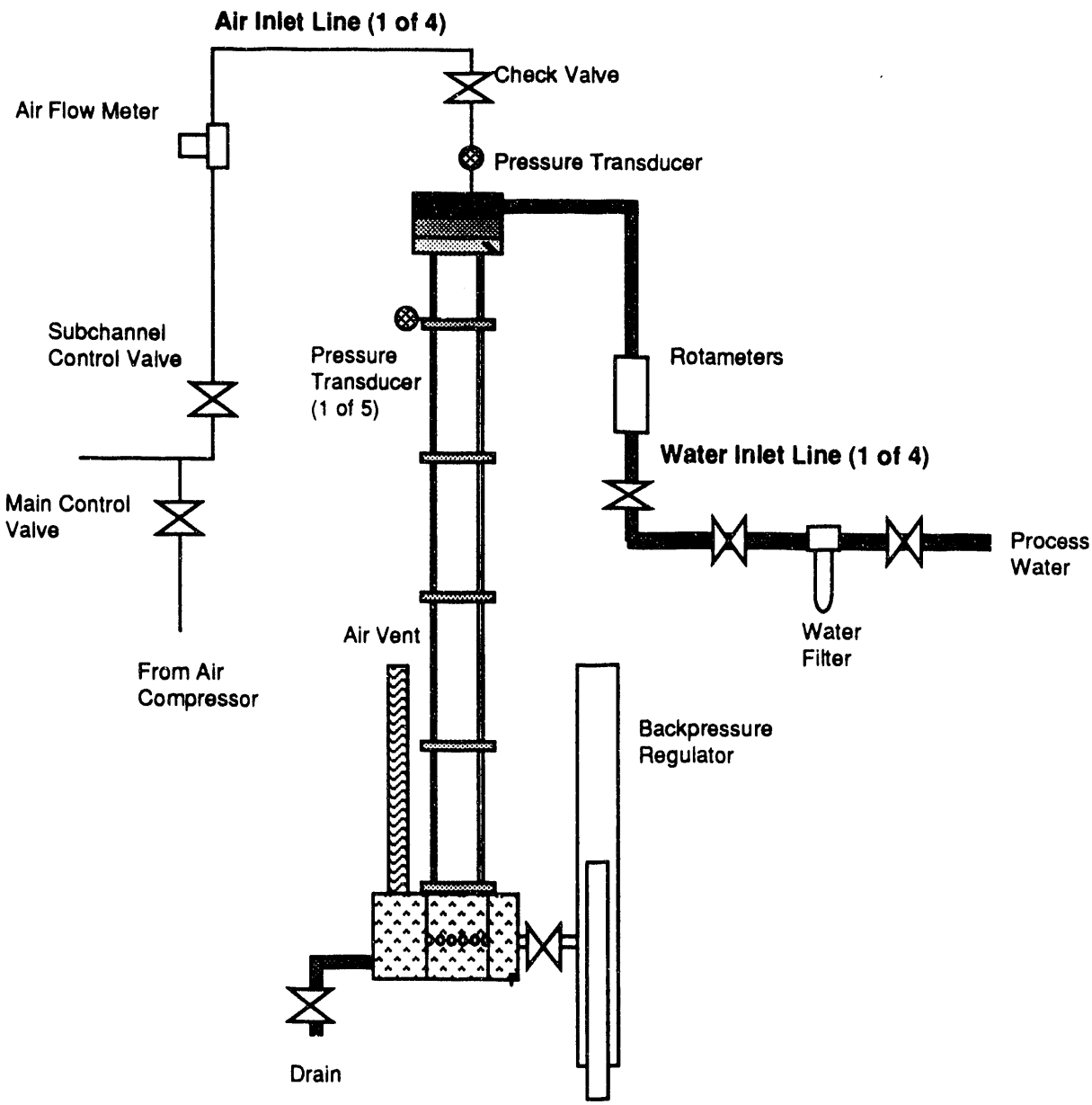

Figure 3
Flow Regime Map: Comparison to Transitions of Barnea et al

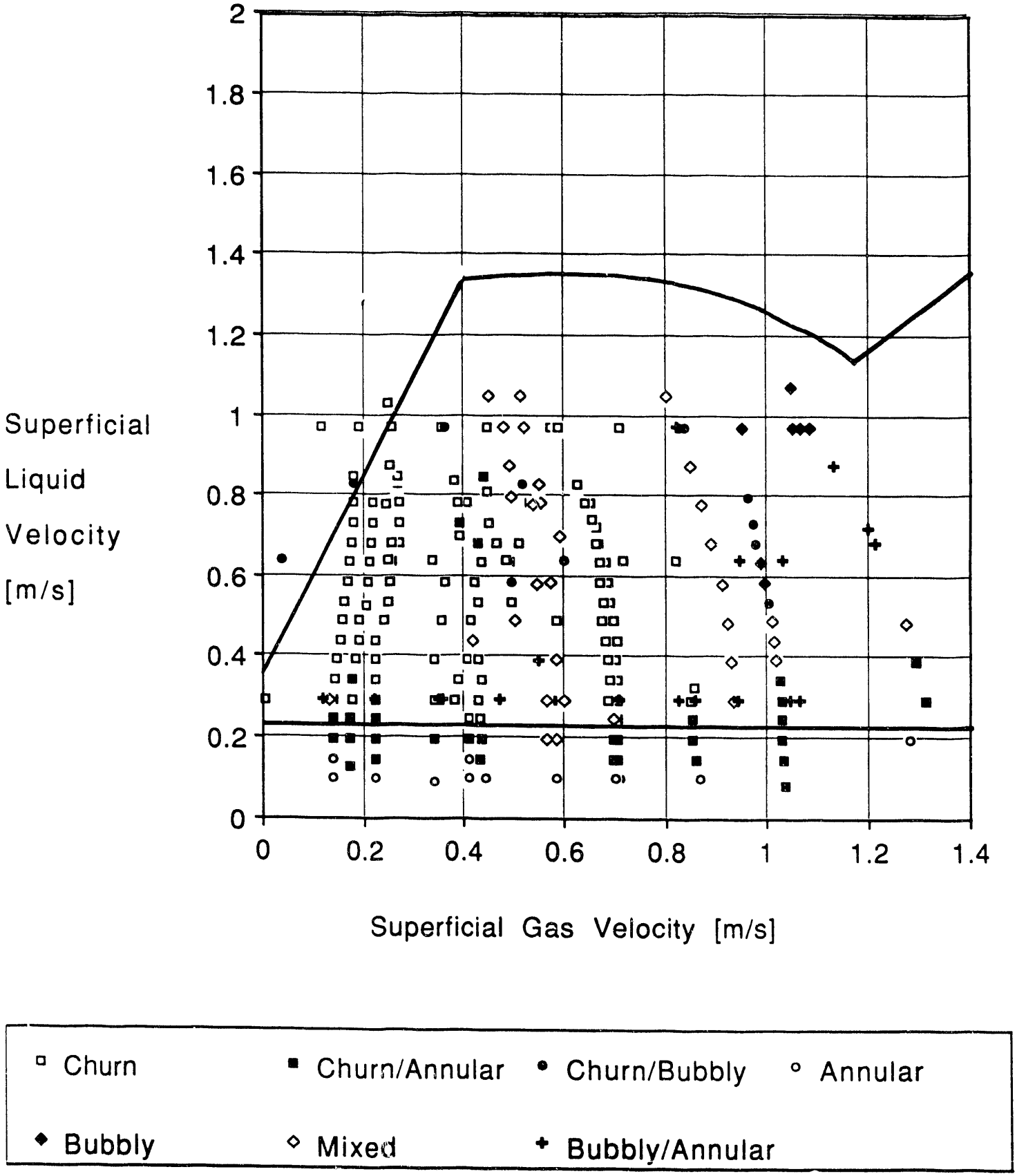

Figure 4
Hysteresis Effects on Flow Map for Ribbed Annulus Downflow:
Superficial Gas Velocity [m/s] vs. Superficial Liquid Velocity [m/s]

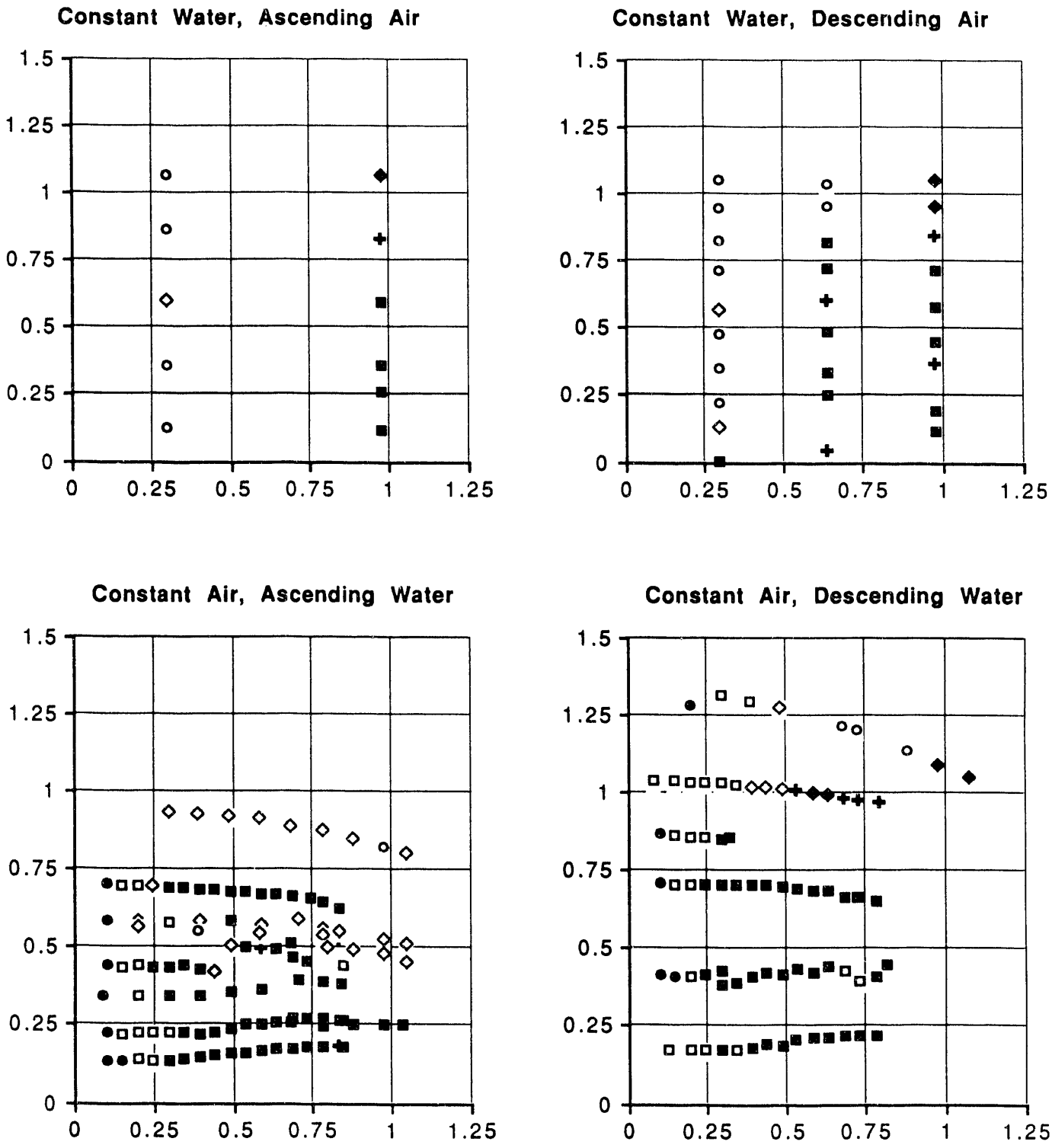

Figure 5
Flow Regime Map: $\sqrt{Fr}$ vs. Volumetric Flow Ratio

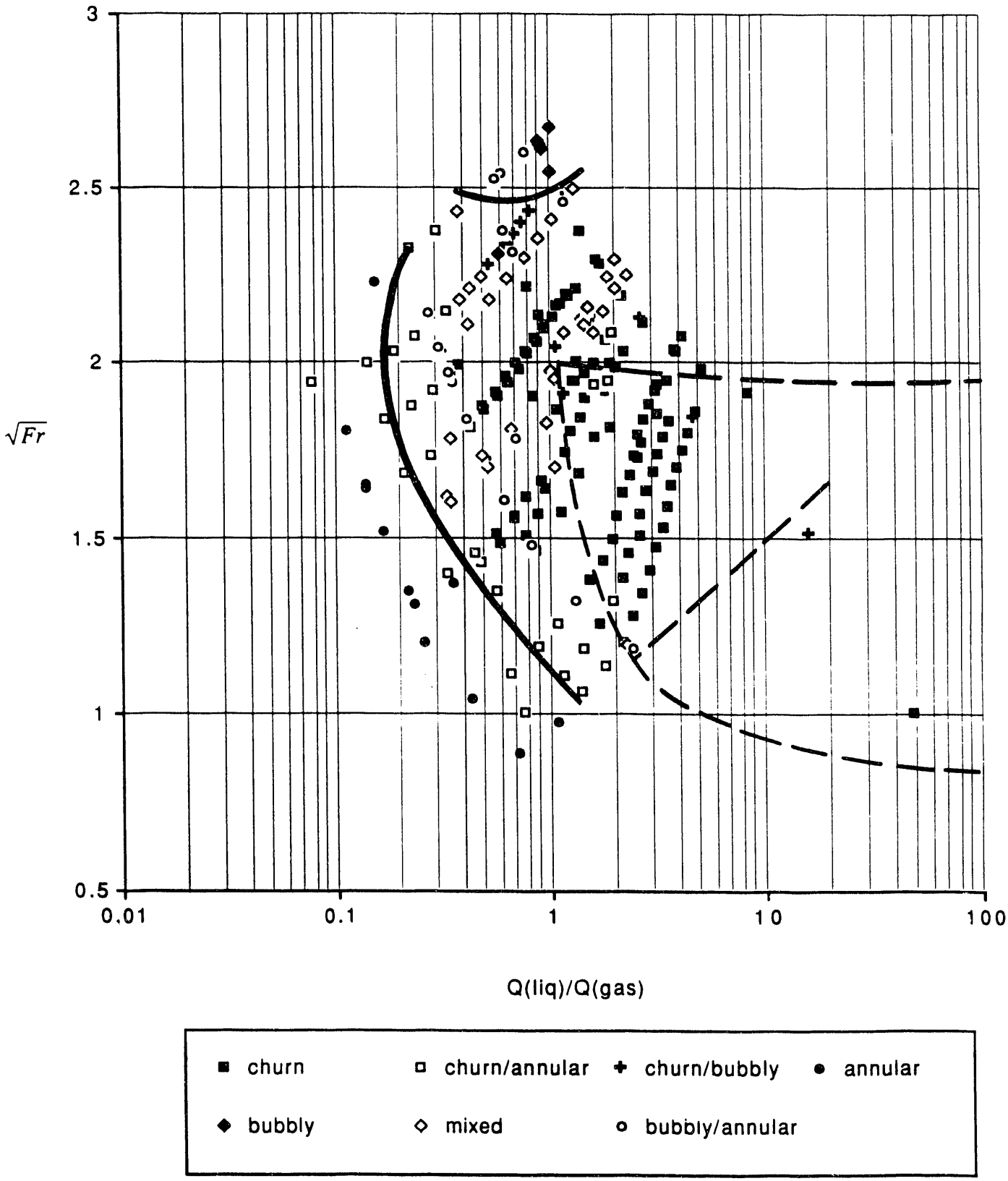

Figure 6
Flow Map in Terms of Void and Total Mass Flux

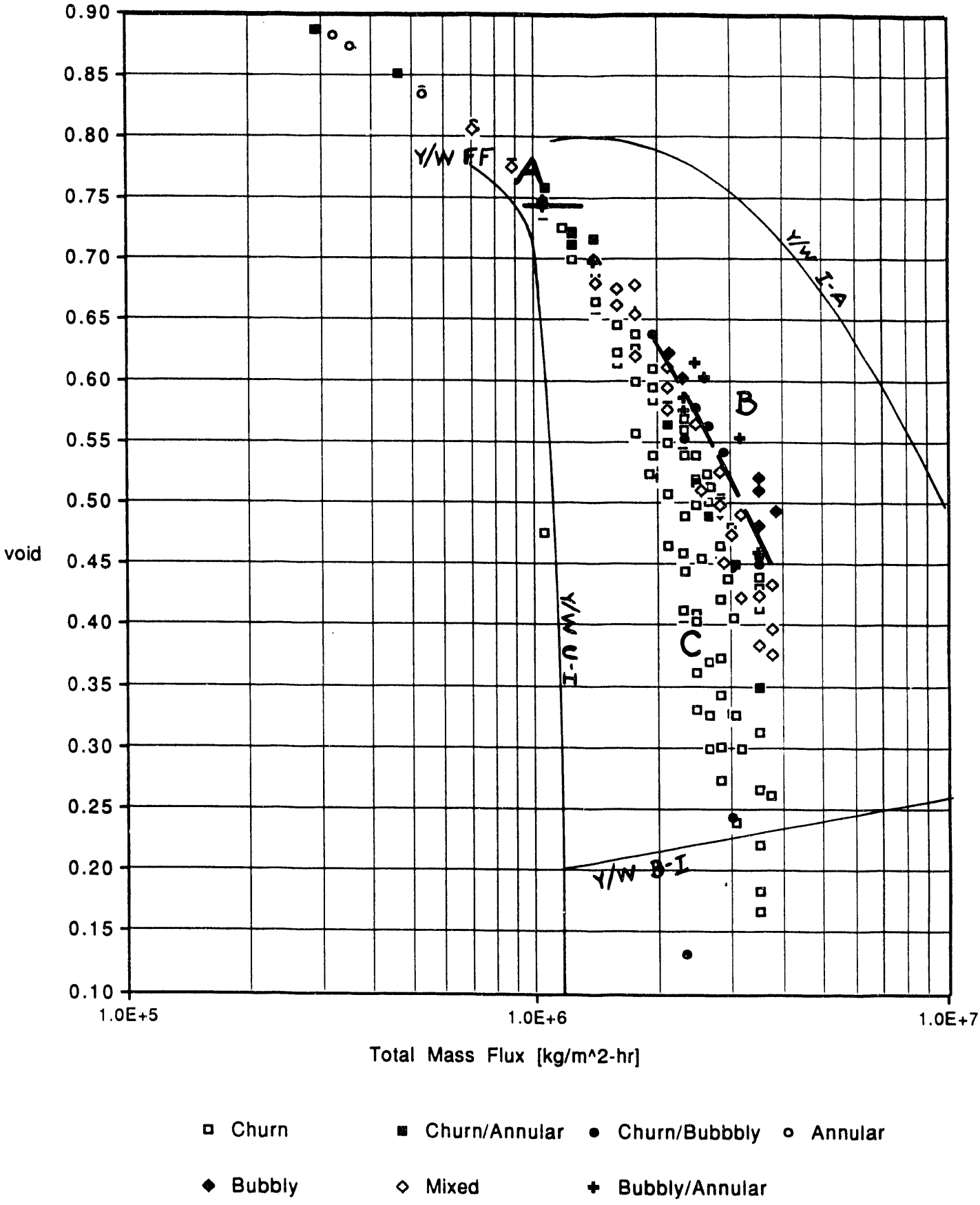

Figure 7
Rise Velocity as a Function of Bubble Length

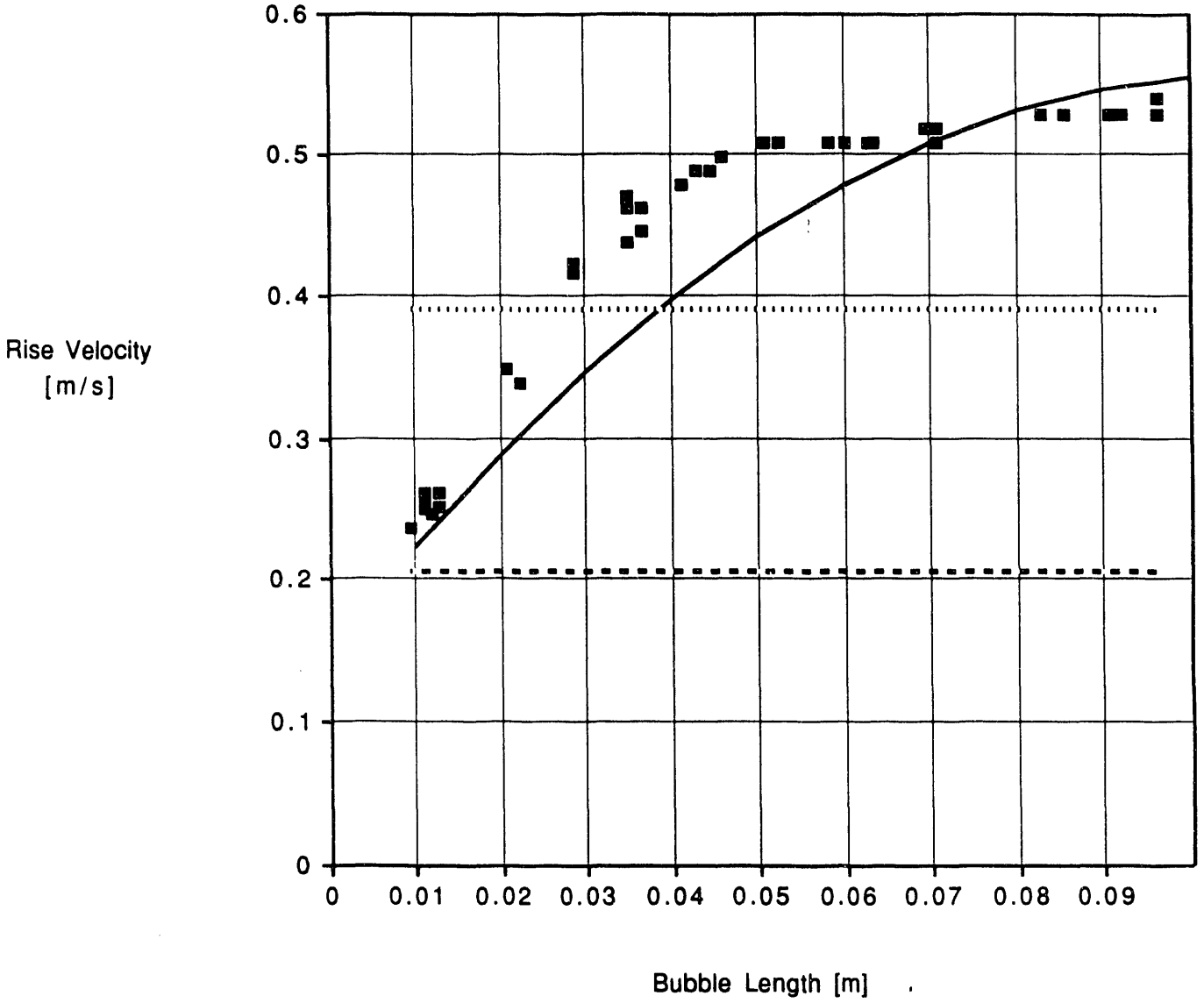

■ experimental values

— elliptical bubble (gamma → 0.5)

▪ ▪ standard form with D = Do/4

···· standard form; Barnea & Shemer expression for D

END

DATE
FILMED
7/9/93